JCI insight

RESEARCH ARTICLE

ICAM1+ neutrophils promote chronic inflammation via ASPRV1 in B cell–dependent autoimmune encephalomyelitis

Ryder F. Whittaker Hawkins,[1] Alexandre Patenaude,[1] Aline Dumas,[1] Rajiv Jain,[2] Yodit Tesfagiorgis,[2] Steven Kerfoot,[2] Takeshi Matsui,[3] Matthias Gunzer,[4] Patrice E. Poubelle,[5] Catherine Larochelle,[6] Martin Pelletier,[5] and Luc Vallières[1]

[1]Neuroscience Unit, University Hospital Center of Quebec – Laval University, Quebec City, Quebec, Canada. [2]Department of Microbiology and Immunology, Western University, London, Ontario, Canada. [3]Laboratory for Skin Homeostasis, RIKEN Center for Integrative Medical Sciences, Kanagawa, Japan. [4]Institute for Experimental Immunology and Imaging, University Hospital, University Duisburg-Essen, Essen, Germany. [5]Infectious and Immune Disease Unit, University Hospital Center of Quebec – Laval University, Quebec City, Quebec, Canada. [6]Neuroimmunology Research Laboratory, University of Montreal Hospital Research Center, Montreal, Quebec, Canada.

Neutrophils contribute to demyelinating autoimmune diseases, yet their phenotype and functions have been elusive to date. Here, we demonstrate that ICAM1 surface expression distinguishes extra- from intravascular neutrophils in the mouse CNS during experimental autoimmune encephalomyelitis (EAE). Transcriptomic analysis of these 2 subpopulations indicated that neutrophils, once extravasated, acquire macrophage-like properties, including the potential for immunostimulation and MHC class II–mediated antigen presentation. In corroboration, super-resolution (3D stimulated emission-depletion [STED]) microscopy revealed neutrophils forming synapses with T and B cells in situ. Further, neutrophils specifically express the aspartic retroviral-like protease ASPRV1, which increases in the CNS during EAE and severe cases of multiple sclerosis. Without ASPRV1, mice immunized with a new B cell–dependent myelin antigen (but not with the traditional myelin oligodendrocyte glycoprotein peptide) develop a chronic phase of EAE that is less severe and even completely fades in many individuals. Therefore, ICAM1+ macrophage–like neutrophils can play both shared and nonredundant roles in autoimmune demyelination, among them perpetuating inflammation via ASPRV1.

Introduction

People with demyelinating autoimmune diseases, such as multiple sclerosis (MS), neuromyelitis optica spectrum disorder (NMOSD), and acute disseminated encephalomyelitis (ADEM), have a corrupted immune system that destroys the myelin sheath of neurons in the CNS. The root causes of these diseases remain unknown, but the underlying molecular and cellular mechanisms are fairly well comprehended, owing to the animal model experimental autoimmune encephalomyelitis (EAE). EAE can be induced in mice by immunization with different myelin antigens (e.g., myelin oligodendrocyte glycoprotein [MOG]) (1). Similarly to its human counterparts, EAE can comprise 5 phases: (i) a preclinical induction phase, in which $CD4^+$ Th cells are primed in lymphoid organs by antigen-presenting cells (e.g., DCs, B cells) and traffic toward the CNS (2); (ii) an onset phase, in which Th cells are licensed at the CNS interface to enter the parenchyma and initiate inflammation (3); (iii) an acute attack phase, in which myeloid cells (e.g., macrophages) execute effector functions resulting in demyelination (4); (iv) a recovery phase, in which immunoregulatory cells act to resolve inflammation either partially or completely (5); and (v) a chronic phase, in which corrupted immune cells succeed in perpetuating the inflammation. The mechanism responsible for the progression of acute to chronic inflammation is unknown yet critical for understanding and treating autoimmune diseases.

The past decade of research has unmasked a new player in autoimmune demyelination: the neutrophil granulocyte. As discussed in a recent review (6), this type of myeloid cell is observed in the CNS during

Authorship note: RFWH and AP contributed equally to this work.

Conflict of interest: LV is listed as an inventor on a provisional patent application (US no. 62/533,398) filed by Laval University for the use of ASPRV1 as a biomarker and therapeutic target.

Submitted: August 14, 2017
Accepted: October 23, 2017
Published: December 7, 2017

Reference information:
JCI Insight. 2017;2(23):e96882.
https://doi.org/10.1172/jci.insight.96882.

NMOSD, ADEM, and severe forms of MS. In the most common forms of MS, neutrophils are typically absent from brains taken at autopsy, usually many years after diagnosis. However, one study reports their presence in the cerebrospinal fluid of early-diagnosed MS patients (7), and several indirect observations link neutrophils to the most common forms of MS (6). In EAE pathogenesis, the importance of neutrophils is clear: the disease can be blocked or attenuated by depleting neutrophils or molecules involved in their recruitment (6). However, their exact functions remain elusive, in part because their phenotype has not yet been characterized and because there is a paucity of biomarkers and genetic deletion tools for neutrophil assessment.

In the present study, we show that neutrophils that infiltrate the spinal cord parenchyma during EAE, but not intravascular neutrophils that crawl on the luminal endothelial surface, bear on their surface the adhesion molecule ICAM1 (CD54). Using this marker, we isolated these 2 neutrophil populations and compared their transcriptomes in order to gain insights into their properties. The results suggest that neutrophils, in EAE, exert macrophage-like functions, as well as a specific effect via the enzyme aspartic peptidase retroviral-like 1 (ASPRV1, also known as SASPase). ASPRV1 is synthesized as a zymogen that contains a putative transmembrane domain and a conserved catalytic domain with a key aspartic acid residue (8–10). This zymogen can undergo autocleavage under slightly acidic conditions, releasing the catalytic domain that homodimerizes to form an active protease (8, 9). ASPRV1 has so far only been detected in stratified epithelia, where it cleaves its only known substrate, profilaggrin (8, 9, 11, 12). Its knockdown or overexpression causes no major physiological defect (although the skin of adult ASPRV1-deficient mice shows fine wrinkles and reduced hydration) (9, 11, 12). Here, we demonstrate that ASPRV1 is: (i) only expressed by neutrophils in the immune and nervous systems both in mice and humans and (ii) essential for the progression of acute to chronic inflammation, specifically when EAE is induced with a new MOG antigen that involves — like in MS (13) and contrary to the traditional $MOG_{35–55}$ peptide (14) — a deleterious action of B cells.

Results

ICAM1 distinguishes extra- from intravascular neutrophils in the CNS of EAE mice. To study the phenotype of neutrophils in EAE, cell-surface markers (CD45, CD11b, Ly6G, ICAM1) were analyzed by flow cytometry in the spinal cord and blood of mice immunized with $MOG_{35–55}$ and adjuvants (i.e., complete Freund's adjuvant and pertussis toxin). Sham-immunized mice (adjuvants only) and naive mice were used as controls. Samples were taken at day 15 after immunization — a time point at which all mice had developed signs of EAE (clinical scores ranging from 0.5–3; mean, 1.9 ± 0.2) and at which neutrophils were expected to be mobilized to the CNS (15–17).

As shown in Figure 1, A and B, neutrophils ($CD45^+CD11b^+Ly6G^+$) were expanded in the spinal cord and blood of both EAE mice and sham-immunized mice relative to naive controls. While this cell expansion in the blood was comparable between these 2 groups, it was 4.3 times higher in the CNS of EAE mice relative to sham-immunized mice (Figure 1B). These results are consistent with the prior observation that neutrophils crawl more frequently on the CNS endothelial surface upon exposure to adjuvants (16, 18, 19) but infiltrate the parenchyma only during EAE (15–17).

Interestingly, ICAM1 was highly expressed (median fluorescence intensity [MFI], 2,052 ± 510) on a large proportion of spinal cord neutrophils (64% ± 9%) in EAE, but not in sham (Figure 1, C and D, upper panels). ICAM1 was generally not expressed on blood neutrophils, except at low levels (MFI, 84 ± 5) and on a small proportion (13% ± 3%) in EAE and sham (Figure 1, C and D, lower panels). In the spinal cord, $ICAM1^+$ neutrophils expressed higher levels of CD11b and CD45 than did $ICAM1^–$ neutrophils (Figure 2A). Both populations were identical on the basis of their forward and side scatter properties (data not shown) and nuclear morphologies (Figure 2, B and C). Similar observations were made at other time points (e.g., day 12, 24) and in brain samples (data not shown).

To facilitate the anatomical localization of $ICAM1^+$ and $ICAM1^–$ neutrophils, we generated reporter mice with green fluorescent neutrophils by crossing heterozygous Catchup mice (20) (expressing Cre recombinase under the neutrophil-specific *Ly6g* promoter) with Ai6 mice (21) (expressing ZsGreen fluorescent protein permanently upon Cre activity). Spinal cords were collected for confocal imaging 15 days after EAE induction. In general, $ZsGreen^+$ neutrophils (with characteristic multilobed nuclei) were concentrated in inflammatory foci near the central canal and in meningeal and submeningeal areas of the spinal cord (Figure 3A). These cells were confirmed to be neutrophils by colocalization of ZsGreen with Ly6G (Figure 3B). ICAM1 was detected on capillaries but not on intravascular neutrophils that exhibited the rod-shaped

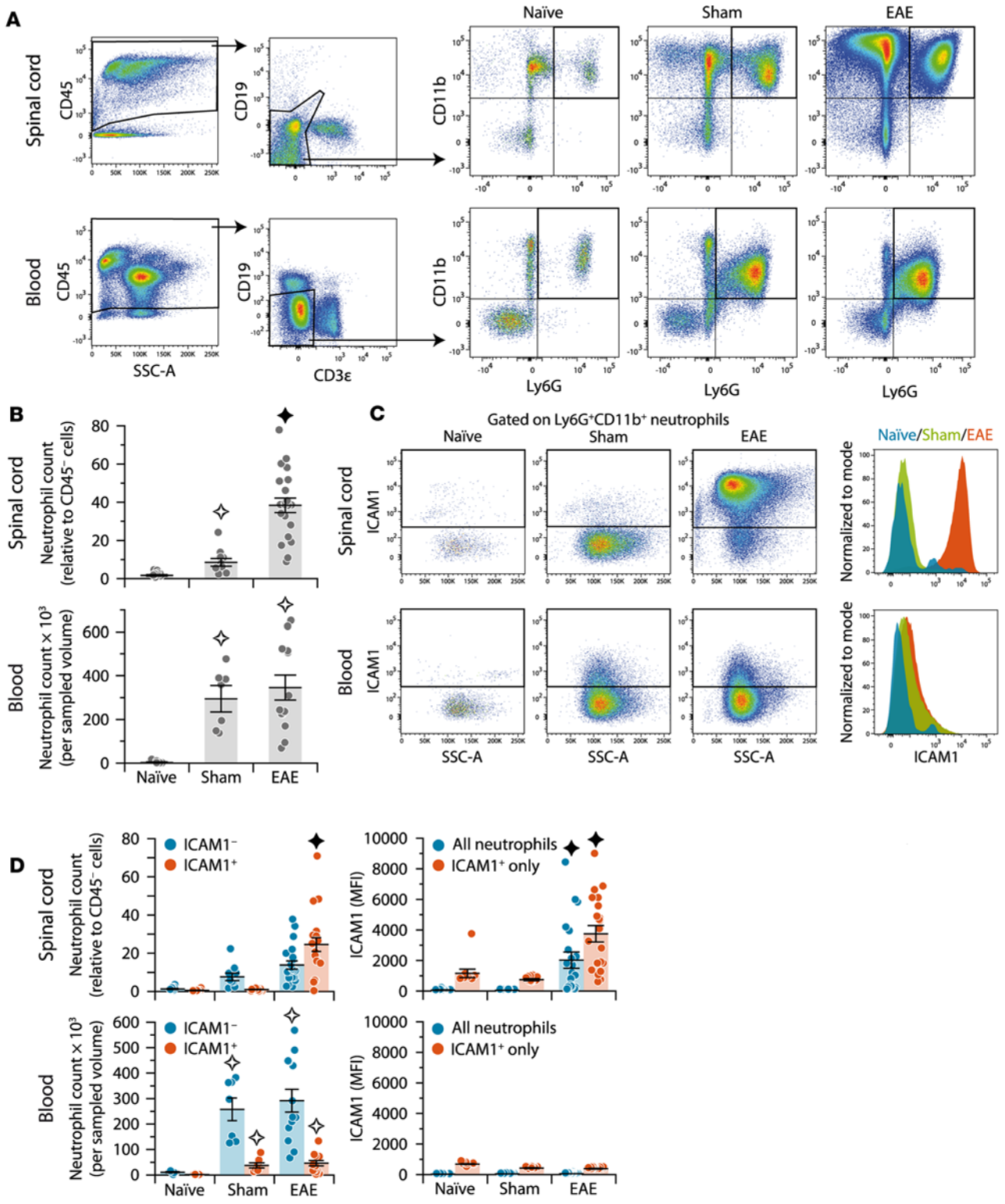

Figure 1. The spinal cord of EAE mice contains 2 subsets of neutrophils distinguishable by ICAM1 surface expression. (**A**) Flow cytometry gating strategy used to analyze neutrophils ($CD45^+CD11b^+Ly6G^+CD19^-CD3\varepsilon^-$) from the spinal cord or blood of mice euthanized 15 days after immunization either with or without MOG_{35-55} (EAE or sham, respectively). Naive mice were used as additional controls. Dead cells and doublets were excluded. (**B**) Quantification of the data in **A** revealing an increase of neutrophils in the spinal cord and blood of EAE and sham-treated mice. For the spinal cords, counts were normalized to $CD45^-$ cells as an internal control. Stars indicate significant increases from both the naive and sham-treated mice (closed star) or from the naive mice only (open star), as determined by 2-way ANOVA and post hoc 2-tailed Student's *t* test ($P \leq 0.0089$). Sample size for spinal cord: 21 (EAE), 10 (sham, naive). Sample size for blood: 13 (EAE), 7 (sham), 6 (naive). (**C**) Cytometric analysis of ICAM1 on neutrophils from the spinal cord or blood of EAE and control

mice. Data were gated as in **A**. (**D**) Quantification of the data in **C** revealing a strong increase of ICAM1 expression on neutrophils isolated from the spinal cord of EAE mice. Left charts, counts of ICAM1$^+$ and ICAM1$^-$ neutrophils in the spinal cord and blood. Right charts, median fluorescence intensity (MFI) obtained for ICAM1 when gated on the whole population of neutrophils or only on those positive for ICAM1. Stars indicate significant increases of ICAM1$^+$ neutrophils from both the naive and sham-treated mice (closed star) or from the naive mice only (open star), as determined by 2-way ANOVA and post hoc 2-tailed Student's *t* test ($P \leq 0.0016$). Sample size as in **B**.

morphology typical of crawling leukocytes (ref. 22 and Figure 3C). In contrast, ICAM1 was detected on the vast majority (>90%) of extravascular neutrophils in the meninges and parenchyma (Figure 3D). Neutrophils were also observed in the vasculature of naive and sham-treated mice (where they were negative for ICAM1) but never in the parenchyma, as previously reported (18, 19).

We conclude the existence of 2 populations of neutrophils in the CNS of EAE mice: one patrols the CNS vasculature by crawling on its inner surface and is characterized by the absence or very low levels of ICAM1; the other, more abundant, is recruited into the meninges and parenchyma by an antigen-driven mechanism and is characterized by strong expression of ICAM1 and higher levels of CD11b and CD45. This phenotype suggests a state of increased activation (23, 24). We propose that circulating ICAM1$^-$ neutrophils (nonactivated) have the potential to transmigrate across the CNS vasculature and to mature into ICAM1$^+$ neutrophils (activated) that contribute to EAE development.

ICAM1$^+$ neutrophils have a distinctive transcriptional profile revealing a potential for antigen presentation and immunostimulation. To compare the transcriptomes of ICAM1$^+$ and ICAM1$^-$ neutrophils (CD45^{hi}CD11b$^+$CD11c$^-$Ly6G$^+$), we purified these cells by FACS from the spinal cord of EAE mice at day 15 after immunization. For comparison, we simultaneously purified 2 other subsets of myeloid cells: macrophages (CD45^{hi}CD11b$^+$CD11c$^-$Ly6G$^-$) and DCs (CD45^{hi}CD11b$^+$CD11c$^+$Ly6G$^-$). RNA was analyzed in biological duplicate using Affymetrix GeneChip Mouse Gene 2.0 ST arrays interrogating 28,137 coding transcripts (Supplemental Table 1; supplemental material available online with this article; https://doi.org/10.1172/jci.insight.96882DS1). Raw and processed data have been deposited in the ArrayExpress database at EMBL-EBI (www.ebi.ac.uk/arrayexpress) under accession number E-MTAB-6160.

Unsupervised hierarchical clustering revealed that the transcriptome of ICAM1$^+$ neutrophils was substantially different from that of ICAM1$^-$ neutrophils (Figure 4A). Among the 479 genes that were differentially expressed between these cells according to stringent criteria (fold change ≥ 3, mean hybridization signal ≥ 200 in at least 1 subset, $P \leq 0.05$), 343 were upregulated and 136 were downregulated in ICAM1$^+$ neutrophils (Figure 4A and Supplemental Tables 2 and 3). Hence, neutrophils are functionally plastic in EAE: after extravasation into the inflamed CNS, they acquire distinct properties through a substantial transcriptional remodeling.

Hierarchical clustering also showed that ICAM1$^+$ neutrophils were more similar to macrophages and DCs than ICAM1$^-$ neutrophils were (see dendrogram in Figure 4A). Of the 343 genes that were upregulated in ICAM1$^+$ neutrophils (Supplemental Table 2), 328 (96%) were also expressed by macrophages and/or DCs at similar or higher levels. Further, 232 (68%) had a known function and could be manually divided into 12 functional categories, including cell-cell or cell-matrix interaction, cytokine-cytokine receptor interaction, and antigen presentation (Figure 4B). These 3 latter categories also stood out as overrepresented when the classification was done with software tools (KEGG and Ingenuity Pathway Analysis, $P < 0.0001$). Notably, they included many genes coding for cytokines (e.g., IL-1α, CSF1), leukocyte chemoattractants (e.g., CXCL9-11, CCL2-5), cell-surface receptors (e.g., CCR2, CCR5, HAVCR2, NIACR1), and adhesion molecules (e.g., VCAN) (Figure 4C). Remarkably, ICAM1$^+$ neutrophils upregulated molecules at every step along the antigen-processing and -presentation pathway (Figure 4C): proteases that intracellularly process protein antigens (e.g., LGMN, IFI30, CTSB); subunits of the immunoproteasome (e.g., PSMB10); chaperones necessary for MHCII complex formation (e.g., CD74/Ii, H2-DMa); MHCII subunits themselves (H2-Aa, H2-Ab1, H2-Eb1); and costimulatory molecules (e.g., CD40, CD48, CD83, CD86). By flow cytometry, the presence of MHCII and costimulatory molecules was confirmed on a considerable proportion of ICAM1$^+$ neutrophils: 12.5% expressed high levels of MHCII with costimulatory molecules, 50.7% expressed moderate levels of MHCII, and 36.8% were MHCII$^-$ (Figure 5). These results indicate that neutrophils, after infiltrating the CNS, acquire macrophage/DC properties, including the potential ability to secrete immunostimulatory factors and present antigen to lymphocytes (Figure 4, E and F).

Another 104 genes were predominantly expressed in neutrophils and either not expressed or weakly expressed in the other myeloid cells (Figure 4A and Supplemental Table 4). Those that were expressed in both neutrophil subsets included genes coding for well-known neutrophil markers (e.g., Ly6G, CXCR2,

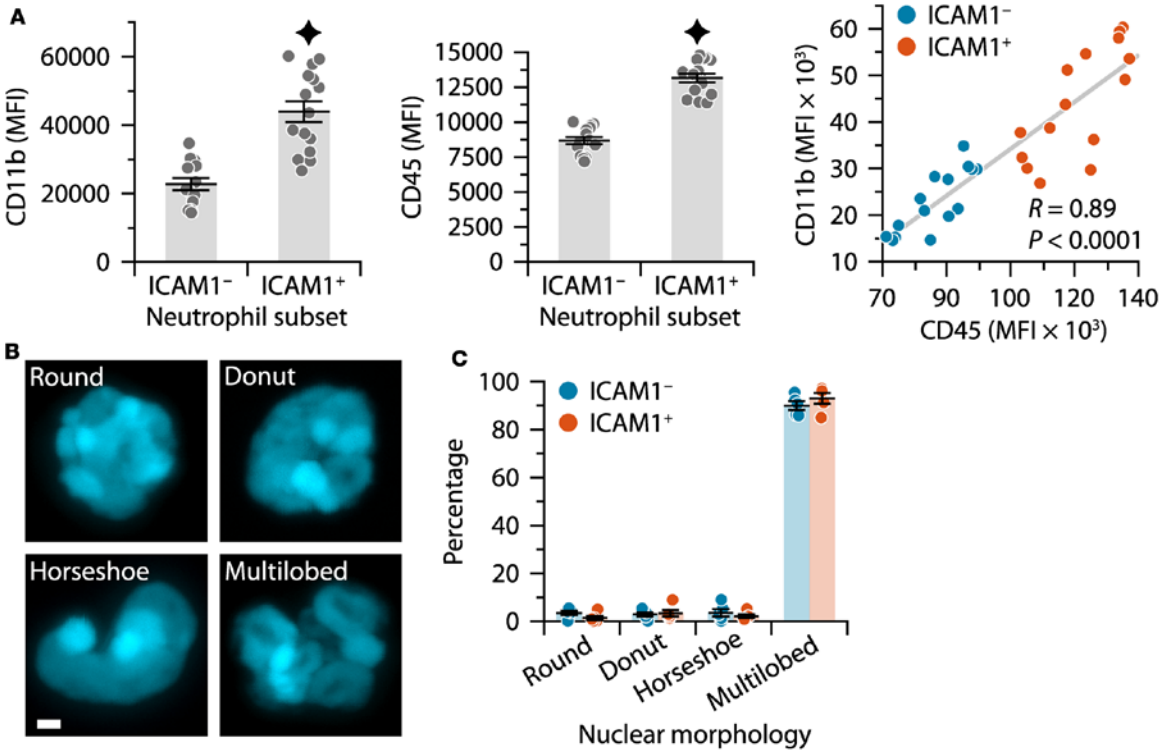

Figure 2. Further characterization of ICAM1⁺ and ICAM⁻ spinal cord neutrophil populations. (**A**) Flow cytometric quantification of CD11b and CD45 on ICAM1⁺ and ICAM1⁻ neutrophils from the spinal cord of EAE mice. Stars indicate significant increases (2-tailed Student's *t* test, $P < 0.0001$). The right chart shows a positive correlation between CD11b and CD45 expression (Pearson correlation test). $n = 15$ per group. (**B**) Confocal images showing different nuclear morphologies in spinal cord neutrophils isolated by FACS and stained with DAPI. Scale bar: 1 μm. (**C**) Frequency of the different nuclear morphologies in ICAM1⁺ and ICAM1⁻ neutrophils separately purified from the spinal cord of EAE mice by FACS. No intergroup difference was observed (2-tailed Student's *t* test, $P \geq 0.1$). Fifty to 160 nuclei were counted per cell subset and per mouse (total of 5 mice).

MMP9), the recently discovered neutrophil cytokine IL-36γ (25) (also called IL1F9), the enzyme histidine decarboxylase (HDC) that synthesizes histamine, and new potential neutrophil markers with unclear functions (e.g., ASPRV1, CHI3L1) (Figure 4D). Thirteen of these 104 genes, notably melanoregulin (*Mreg*) and *IL23a* (Figure 4D), were enriched ≥ 3-fold in ICAM1⁺ neutrophils compared with ICAM1⁻ neutrophils. Thus, it appears that neutrophils are equipped with a specific set of molecules, allowing them to execute unique functions in EAE, in addition to roles redundant with those of macrophages and DCs.

ICAM1⁺ neutrophils do not differentiate into Ly6G⁻ monocytic cells. Our microarray and quantitative PCR (qPCR) data revealed that *Ly6g* mRNA was ~5 times less abundant in ICAM1⁺ neutrophils compared with ICAM1⁻ neutrophils (Figure 6, A and B). This observation prompted us to examine whether Ly6G was uniformly distributed among the 3 subpopulations of neutrophils defined by the levels of MHCII. Flow cytometric analysis revealed that Ly6G expression was roughly similar on MHCII⁻ and MHCII^{mid} neutrophils, but 3-fold lower on MHCII^{hi} neutrophils (Figure 6C).

An intriguing question arises as to whether MHCII^{hi}Ly6G^{lo} neutrophils ultimately go on to lose Ly6G completely. If this were correct, then gating our samples on Ly6G as a neutrophil marker would lead to underestimating the number of infiltrating neutrophils and to excluding a potentially important neutrophil subset. The possibility that neutrophils become negative for Ly6G is supported by an independent study showing that neutrophils can differentiate into Ly6G⁻ monocytic cells under inflammatory conditions in vivo (26). To test this possibility in EAE, we permanently labeled neutrophils using the Catchup × Ai6 model (described above) and analyzed them by flow cytometry. Approximately 80% of all Ly6G⁺ neutrophils from the spinal cord of EAE mice expressed ZsGreen. Curiously, Ly6G⁺ neutrophils accounted for 78% of the ZsGreen⁺ population, while the remaining 22% were other myeloid phagocytes: DCs, macrophages, and microglia (Figure 6D).

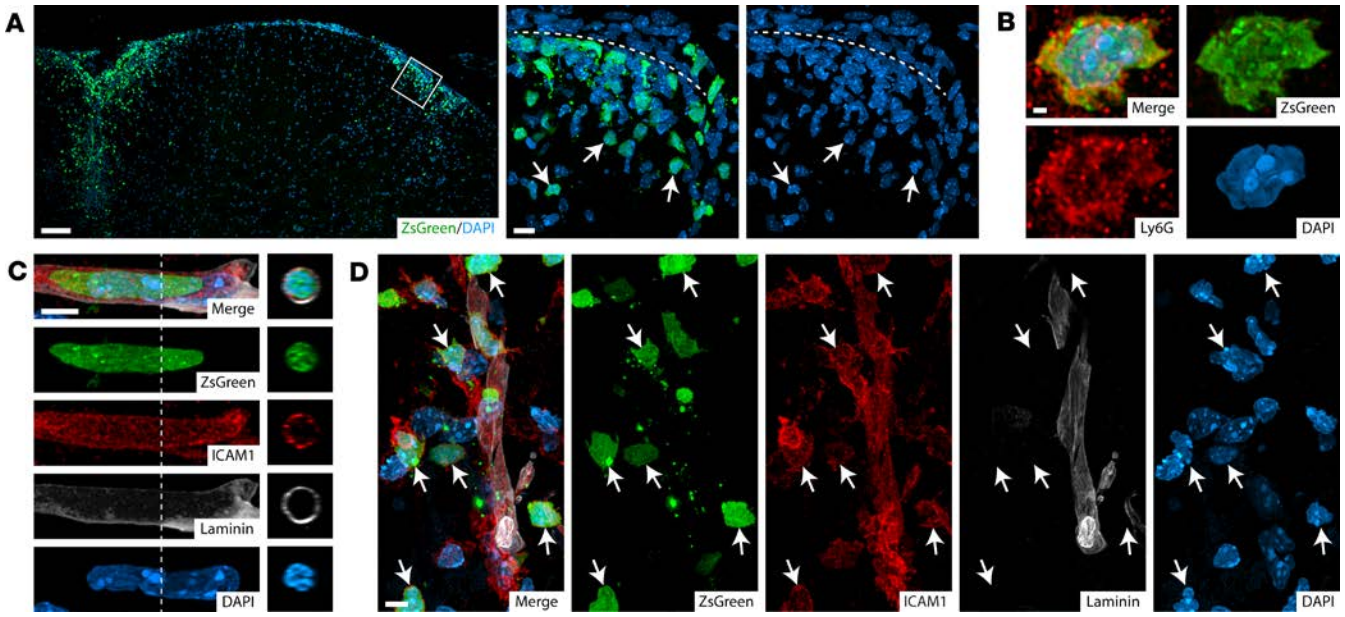

Figure 3. ICAM1⁺ and ICAM1⁻ neutrophils are differently distributed in the spinal cord during EAE. (**A**) Confocal images of a spinal cord section from a Catchup × Ai6 mouse with EAE (day 15) showing ZsGreen⁺ neutrophils (arrows) infiltrated in meningeal and submeningeal inflammatory foci. Note the multilobed morphology of their nucleus stained with DAPI. The right images are higher magnification views of the box in the left image. The dashed line delineates the leptomeninges. Scale bar: left, 100 μm; right, 10 μm. (**B**) High magnification of a ZsGreen⁺ neutrophil immunostained for Ly6G. Scale bar: 5 μm. (**C**) An ICAM1⁻ neutrophil with a rod-shaped morphology crawling on the luminal surface of an ICAM1⁺ capillary (white, immunostaining for laminin revealing the endothelial basal membrane). Right images are *y-z* sections taken at the dashed line. Scale bar: 5 μm. (**D**) Extravasated ICAM1⁺ neutrophils with an amoeboid morphology. Scale bar: 5 μm.

To determine whether this latter result was real differentiation or simply attributable to engulfment of ZsGreen⁺ neutrophil debris, we examined spinal cord sections immunostained for Iba1 (also known as AIF1), a marker of microglia and other myeloid phagocytes (27). We found that virtually all cells double-positive for ZsGreen and Iba1 were actually cells containing ZsGreen⁺ debris in their cytoplasm (Figure 6E). However, we did see a few cells that were truly double-positive with ZsGreen throughout the cytoplasm (data not shown); these cells exhibited a multilobed nucleus, expressed lower levels of Iba1 than other myeloid cells (consistent with our microarray data in Supplemental Table 1 revealing Iba1 expression in ICAM1⁺ neutrophils), and accounted for only a minor fraction of ZsGreen⁺ cells (<1%).

Thus, we conclude that ICAM1⁺ neutrophils decrease, but do not lose, their expression of Ly6G during migration into the CNS parenchyma; there, they adopt some macrophage characteristics but do not differentiate into a different myeloid cell type. The diminution of Ly6G expression could still reduce the number of cells estimated by immunofluorescence, due to the lower sensitivity of the technique. Furthermore, flow cytometric analysis of neutrophils in the Catchup × Ai6 model must be done with caution, as a significant proportion of ZsGreen⁺ cells may be contaminated with other myeloid phagocytes that have internalized remnants of dead neutrophils, a phenomenon also observed in stroke (28).

ICAM1⁺ neutrophils form immunological synapses with T and B cells. Our microarray results indicate that infiltrating neutrophils upregulate proteins known to be important for physical and functional interactions with lymphocytes (e.g., ICAM1, MHCII, and costimulatory molecules) (Figure 4 and 5). To determine whether such interactions occur in our model, spinal cord sections from Catchup × Ai6 mice with EAE were stained for CD3ε and B220; then, the number of neutrophils physically contacting lymphocytes was estimated. Figure 7A gives an overview of one such section, where neutrophils and T cells were localized both in the parenchyma and surrounding meninges, whereas most B cells were restricted to the meninges. At higher magnification, we observed — across the tissue — many neutrophils that were juxtaposed to T and B cells (Figure 7B). In all individuals studied (4), these contacts were frequent: in the meninges, for example, approximately 36% of ZsGreen⁺ neutrophils contacted CD3ε⁺ T cells, while another approximately 14% contacted B220⁺ B cells (Figure 7C).

T and B cells can contact antigen-presenting cells (APCs) to form several different types of immunological synapses (29, 30). The most traditional synapse is characterized by a ring of ICAM1 surrounding a central zone devoid of ICAM1 (29). The occurrence of immunological synapses in CNS tissue has

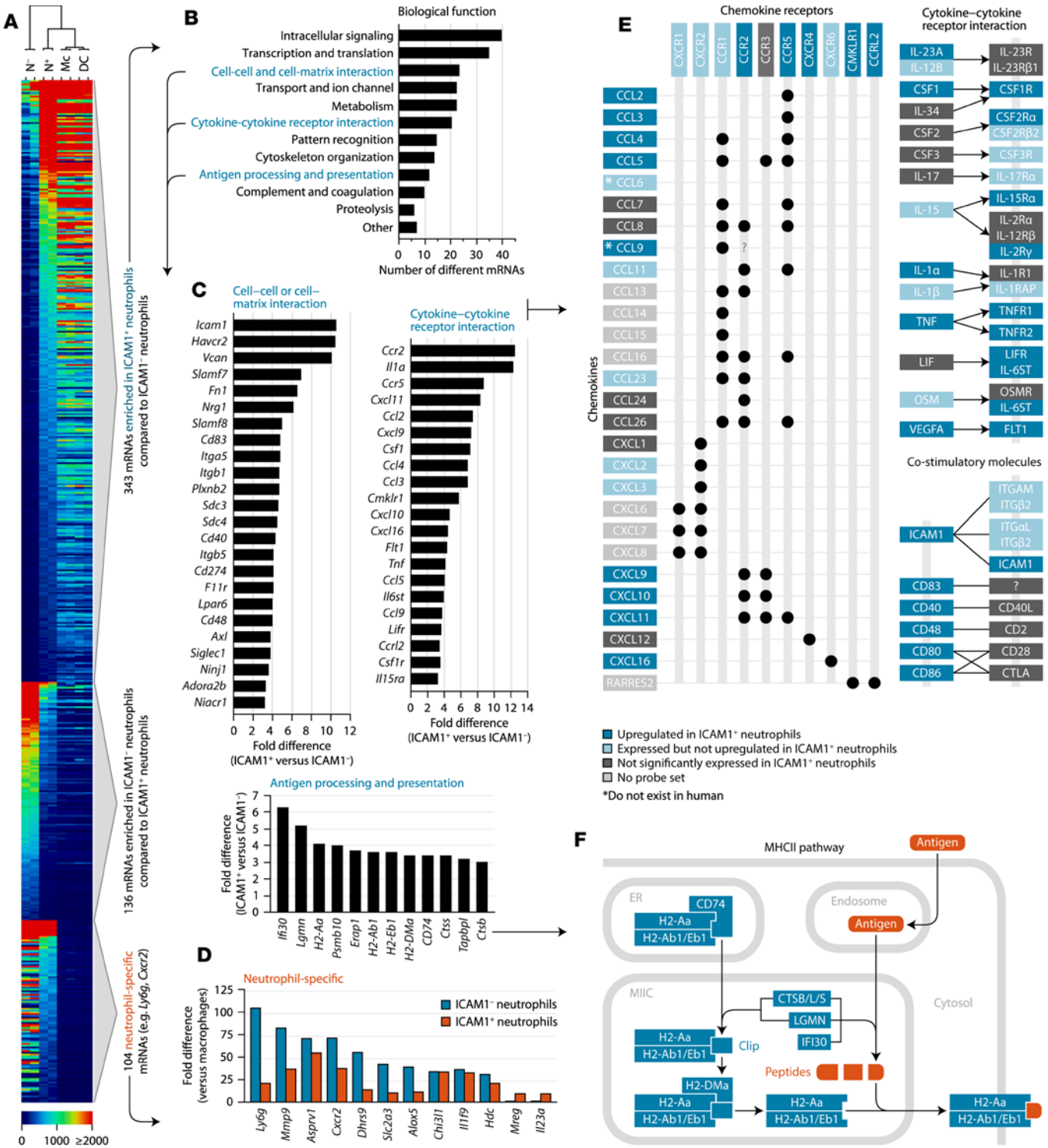

Figure 4. ICAM1⁺ neutrophils have a distinct transcriptional profile suggestive of a capacity for immunomodulation and antigen presentation. (**A**) Heat map of mRNAs differentially expressed in ICAM1⁺ and ICAM1⁻ neutrophils (N^+, N^-) compared with each other or with $CD11b^+CD11c^-Ly6G^-$ macrophages (Mc) and $CD11b^+CD11c^+Ly6G^-$ DC. These cells were simultaneously purified from the spinal cord of EAE mice by FACS and analyzed by DNA microarray. The hierarchical clustering dendrogram shows the degree of similarity among the samples (biological duplicates). The color scale indicates the hybridization signal intensity. The criteria used for comparison were as follows: fold change ≥ 3; hybridization signal ≥ 200; 2-tailed Student's *t* test, $P \leq 0.05$. See Supplemental Tables 1–4 for data sets. (**B**) Frequency distribution, according to biological function, of the 343 mRNAs identified as enriched in ICAM1⁺ neutrophils. (**C**) Fold difference in the hybridization signals for mRNAs of 3 selected categories (blue text in **B**), as compared between ICAM1⁺ and ICAM1⁻ neutrophils. (**D**) Fold difference in the hybridization signals for neutrophil-specific mRNAs, as compared between neutrophils (ICAM1⁺ and ICAM1⁻) and macrophages. (**E**) Signaling proteins expressed (light blue) or upregulated (dark blue) in ICAM1⁺ neutrophils, supporting the concept that these cells acquire immunostimulatory capacities. (**F**) Schematic of the MHCII pathway showing that all of the proteins are upregulated (dark blue) in ICAM1⁺ neutrophils, suggesting the acquisition of antigen-presenting capacity. Color legend as in **E**. MIIC, MHCII compartment.

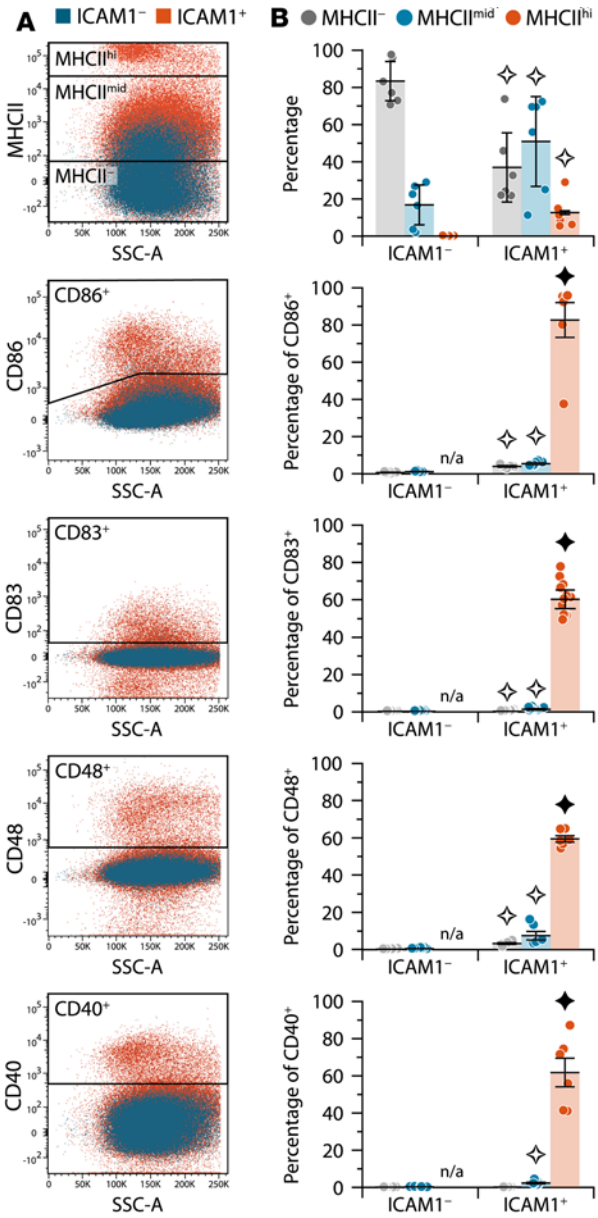

Figure 5. A fraction of ICAM1⁺ neutrophils exhibit surface proteins involved in antigen presentation. (**A**) Representative cytometry plots showing the gates used to analyze MHCII and costimulatory molecules on neutrophils ($CD11b^+Ly6G^+CD11c^-CD19^-CD3\varepsilon^-$) from the spinal cord of EAE mice. Dead cells, debris, and doublets were excluded. (**B**) Quantification of the results in **A** revealing increases of MHCII and costimulatory molecules on subpopulations of $ICAM1^+$ neutrophils. Stars indicate significant differences from the corresponding $ICAM1^-$ population (open star) or from all the other populations (closed star), as determined by the Kruskal-Wallis test and post hoc Wilcoxon test ($P \leq 0.0051$). $n = 13$ mice (CD83), 6 mice (rest).

only been thus far documented between cytotoxic T cells and astrocytes during infection (31, 32). To investigate the fine-scale structure of neutrophil–T cell doublets, we performed super-resolution microscopy by stimulated emission-depletion (STED) with a pulsed depletion beam and time-gated detection (Figure 7D). Three-dimensional reconstructions revealed the presence of a zone devoid of ICAM1 on neutrophils at the plane of contact with T cells (Figure 7E). To our knowledge, this represents the first in vivo evidence that neutrophils form immunological synapses with T cells. Our observations suggest that neutrophils recruited to the mouse CNS during EAE can physically engage with T and B cells and form immunological synapses with T cells, reminiscent of antigen presentation.

To directly test the importance of the antigen-presenting capability of neutrophils in EAE, we crossed Catchup mice to a conditional null strain for H2-Ab1 (33) (the only extant MHCII β–chain allele in C57BL/6 mice and among those genes upregulated in $ICAM1^+$ neutrophils) in order to abolish MHCII expression specifically in neutrophils. Gene deletion (>80%) was confirmed in genomic DNA obtained from spinal cord neutrophils (Supplemental Figure 1A); however, perplexingly, *H2-Ab1* mRNA and protein were unchanged in the same samples (Supplemental Figure 1, B–D). Thus, H2-Ab1 adds to a list of proteins that cannot be studied in the Catchup model (20), perhaps because the deletion is partial, occurs after mRNA transcription, or is bypassed by the acquisition of molecules from other cells (e.g., via trogocytosis or vesicular transfer).

ASPRV1 is specific to neutrophils and increases in the CNS during EAE and severe forms of MS. Seeking to discover a unique function of neutrophils in EAE, we chose to follow up on *Asprv1* because it was the most highly expressed neutrophil-specific gene (Supplemental Table 4) with a human homolog that had not yet been studied in the immune or nervous system, and because it encodes a little-known protease that could play a novel effector role in inflammation. By qPCR, we found that *Asprv1* mRNA was indeed expressed in neutrophils ($ICAM1^+$ and $ICAM1^-$) extracted by FACS from EAE spinal cords but not in any other immune cell types tested (Figure 8A). ASPRV1 protein was also expressed in neutrophils from mouse BM, as revealed by Western blotting with the same antibody used to first detect ASPRV1 in skin (ref. 9 and Figure 8B). Specificity was confirmed by the absence of signal in mononuclear leukocytes and

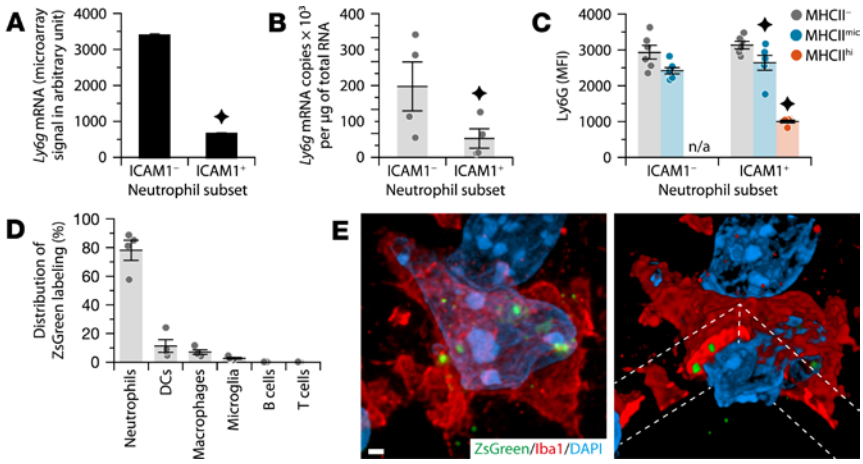

Figure 6. ICAM1⁺MHCII⁺ neutrophils express less Ly6G but do not differentiate into Ly6G⁻ monocytic cells. (**A**–**C**) Quantification of Ly6G expression in neutrophil subsets isolated from the spinal cord of EAE mice at day 14 by microarray, qPCR, or flow cytometry, respectively. Note the reduction of Ly6G expression, which was most pronounced in the MHCII^{hi} fraction. Stars indicate significant decreases from the other group(s) according to 2-tailed Student's *t* test or Wilcoxon test (**A**, $P < 0.0001$; **B**, $P = 0.046$; **C**, $P \leq 0.032$). $n = 2$ (**A**), 4 (**B**), or 6 (**C**) per group. (**D**) Flow cytometric analysis revealing the nature of ZsGreen⁺ cells in the spinal cord of Catchup × Ai6 mice with EAE. ZsGreen expression was analyzed in neutrophils (CD11b⁺Ly6G⁺), DC (CD45^{hi}CD11b⁺CD11c⁺), macrophages (CD45^{hi}CD11b⁺CD11c⁻), microglia (CD45^{lo}CD11b⁺), B cells (CD19⁺), and T cells (CD3ε⁺). (**E**) Deconvolved confocal images of an Iba1⁺ phagocyte (red) containing engulfed ZsGreen⁺ particles. The right image is a 3D reconstruction of the left image with a sliced portion (dashed lines) showing that the ZsGreen⁺ particles are inside the cytoplasm. Scale bar: 1 µm.

Asprv1$^{-/-}$ neutrophils (Figure 8B). In whole spinal cord extracts, *Asprv1* mRNA was barely detectable in the absence of inflammation and upon adjuvant injection (Figure 8C); however, it was highly expressed during EAE and strongly correlated with *Ly6g* mRNA (Figure 8D). The abundance of *Asprv1* mRNA was remarkable (i.e., higher than or equal to *Ly6g* mRNA) both in spinal cord extracts and purified neutrophils (Figure 8D and Supplemental Table 4).

To translate our findings to human, we analyzed, by qPCR, blood fractions and postmortem brain samples from people with or without MS. *ASPRV1* mRNA was abundant in blood neutrophils in the steady state, but not in B cells, Th cells, monocytes, or unfractionated mononuclear cells (Figure 8E). Furthermore, *ASPRV1* mRNA was detected in higher amounts in brain lesions from patients with severe MS compared with both normal-appearing white matter and brain lesions from patients with mild or moderate forms of MS (Figure 8F). Altogether, our results demonstrate that ASPRV1 is a neutrophil-specific protein in the immune system and can serve as a neutrophil marker in the nervous system both in mice and humans.

ASPRV1 is required for the chronic phase of a B cell–dependent EAE model. To determine whether ASPRV1 contributes to EAE, we immunized ASPRV1-deficient and WT mice with 2 different antigens: the standard $MOG_{35–55}$ peptide and bMOG. bMOG is a potentially novel "humanized" mouse $MOG_{1–125}$ protein, developed by members of our group, that bears the S42P mutation abolishing the immunodominant T cell epitope (amino acids 35–55). bMOG can still induce EAE with prominent neutrophilic infiltration, but contrary to MOG peptide (34), it acts through a B cell–dependent mechanism. This was demonstrated in *B1-8*$^{+/+}$*Jκ*$^{-/-}$ mice expressing a single B cell receptor to an irrelevant antigen; these mice did not develop EAE in response to bMOG (Supplemental Figure 2). Therefore, compared with $MOG_{35–55}$, bMOG induces a form of EAE that is more similar to MS, as it involves pathogenic B cells.

After immunization with $MOG_{35–55}$, no difference was observed in EAE incidence and severity between *Asprv1*$^{-/-}$ and WT mice (Figure 9, A and B, and Table 1). In contrast, with bMOG, EAE incidence and acute phase were slightly reduced in the absence of ASPRV1 (Figure 9, A and B, and Table 1). More importantly, the chronic phase was blunted in *Asprv1*$^{-/-}$ mice; after a recovery phase culminating around day 7 after onset, WT mice experienced a relapse, whereas *Asprv1*$^{-/-}$ mice continued to recover, so that 31% of them showed no more clinical signs by the end of experimentation (Figure 9B and Table 1).

To corroborate and explain these symptomatic differences, we performed flow cytometric analysis on spinal cords at different phases of bMOG-induced EAE. At preonset (day 8 after immunization), only

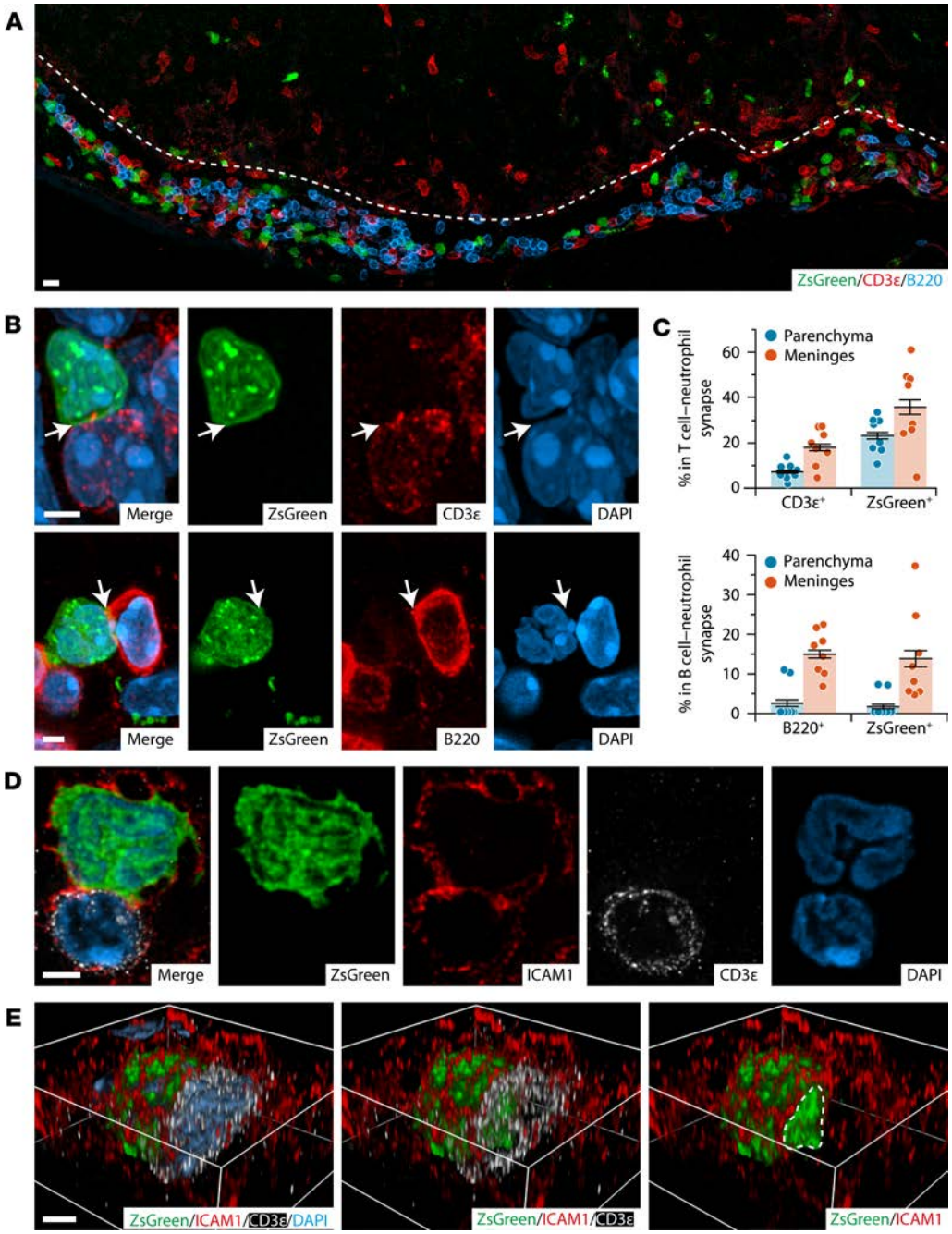

Figure 7. Neutrophils form immune synapses with lymphocytes in the spinal cord of EAE mice. (**A**) Low-magnification confocal image of the spinal cord and meninges in a EAE mouse at day 16 after immunization. Neutrophils (green, ZsGreen) and T cells (red, CD3ε) infiltrated the subpial parenchyma, while B cells (blue, B220) remained in the meninges (under the dashed line). Scale bar: 10 μm. (**B**) Close-up images of neutrophils making synapses (arrows) with T or B cells (top and bottom panels, respectively). Scale bar: 2 μm. (**C**) Frequency of immune synapses in the spinal cord parenchyma and meninges. Data are expressed as the percentage of a given synapse (*y* axis) among a given leukocyte population (*x* axis). *n* = 359–2,167 cells were counted per region per animal (total of 4 EAE mice). (**D**) Super-resolution micrographs of a neutrophil–T cell synapse (only 3 optical sections are shown). ICAM1 and CD3ε were acquired in STED mode, whereas ZsGreen and DAPI were acquired in confocal mode. Scale bar: 2 μm. (**E**) Three-dimensional rendering of the cells in **D** (all optical sections are shown). Note the absence of ICAM1 at the point of synapse (dashed line). Scale bar: 2 μm.

neutrophils and macrophages had begun to accumulate ($P \leq 0.0012$ with respect to naives) but to a similar extent in *Asprv1*$^{-/-}$ and WT mice (Figure 9C). At the peak of EAE (day 13 after induction), all types of infiltrating leukocytes reached their maximal numbers; among them, only macrophages were less numerous in the KOs (by ~46%) (Figure 9C). More precisely, this reduction predominantly affected the ICAM1^{+} subpopulation of macrophages (Figure 9D), which, by analogy with neutrophils, may be presumed to be

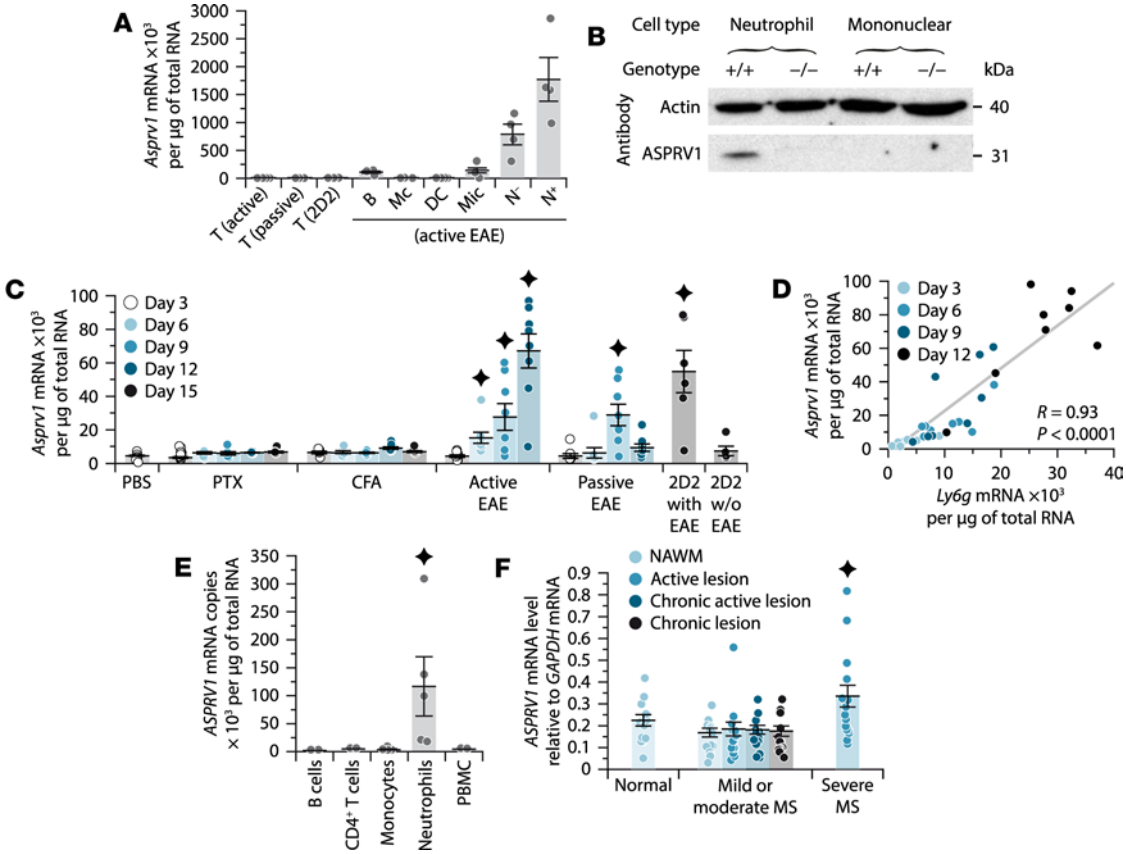

Figure 8. ASPRV1 is a neutrophil-specific marker increased in the CNS during EAE and severe forms of MS. (**A**) Quantification of *Asprv1* mRNA by qPCR in leukocytes isolated by FACS from the spinal cord of EAE mice at day 15 after induction. CD3ε⁺ T cells (T) were from either mice immunized with $MOG_{35–55}$ (active EAE), mice transplanted with encephalitogenic T cells (passive EAE), or 2D2 mice that developed EAE after PTX injection. CD19⁺ B cells (B), CD45^{lo}CD11b⁺ microglia (Mic), CD45^{hi}CD11b⁺CD11c⁺ DC, CD45^{hi}CD11b⁺ macrophages (Mc), and Ly6G⁺ neutrophils expressing or not expressing ICAM1 (N⁺ and N⁻, respectively) were from mice with active EAE. n = 4 per group. (**B**) ASPRV1 protein (~32 kDa) detected by Western blotting in Percoll-enriched neutrophils from the BM of WT mice, but not of *Asprv1*$^{-/-}$ mice or in the mononuclear cell fraction from either genotype. Total loading per well: 20 µg protein. Actin (~42 kDa) was used as a control for protein loading. (**C**) Quantification of *Asprv1* mRNA by qPCR in whole spinal cord from mice with different forms of EAE or from controls (i.e., mice treated with PBS, PTX, or CFA) and 2D2 mice that did not develop EAE after PTX injection (2D2 without EAE). Stars indicate significant differences from PBS, PTX, and CFA (for active and passive EAE) or from 2D2 without EAE (for 2D2 mice) at the same time point (Wilcoxon test, $P < 0.018$). n = 6 (PBS), 7–13 (PTX), 3–8 (CFA), 8 (active EAE), 8 (passive EAE), 6 (2D2 with EAE), and 5 (2D2 without EAE). (**D**) Spearman analysis showing a strong positive correlation between *Asprv1* and *Ly6g* mRNA expression in the spinal cord during active EAE. n = 32. (**E**) qPCR analysis of *ASPRV1* mRNA in freshly isolated human blood cells. Star indicates a significant difference from the other groups (Wilcoxon test, $P = 0.0005$). n = 2–10 per group. (**F**) qPCR analysis of *ASPRV1* mRNA in postmortem brain samples from control individuals (normal) or patients with MS of varying degrees of severity (mild, moderate, or severe). NAWM, normal-appearing white matter. Star indicates a significant difference from the other groups (Wilcoxon test, $P = 0.006$). n = 13–16 per group.

extravasated. A similar reduction (43%) in infiltrating macrophages was estimated by stereology using spinal cord sections stained for F4/80 (WT, 83,969 ± 12,287; KO, 47,954 ± 14,025; 2-tailed Student's t test, $P = 0.040$). No abnormality was noticed in the state of activation of either ICAM1⁺ macrophages or neutrophils, as inferred from their surface levels of CD45, CD11b, ICAM1, MHCII, and CD86 (data not shown). By the chronic phase (day 21 after immunization), many leukocytes (neutrophils, macrophages, DCs) had left the spinal cord of both mouse strains, leaving behind a sizable population of T cells; in *Asprv1*$^{-/-}$ mice, even fewer cells remained, and the number of T cells was only one-sixth that of WT mice (Figure 9C).

The lower sensitivity of *Asprv1*$^{-/-}$ mice to bMOG was not attributable to a defect in neutrophil migration because no substantial intergenotype difference was seen either in the number of ICAM1⁺ neutrophils that had infiltrated the CNS tissue at the peak of EAE (Figure 9D) or in the number of ICAM1⁻ neutrophils crawling inside the CNS vasculature (Figure 9D) or circulating in blood (Figure

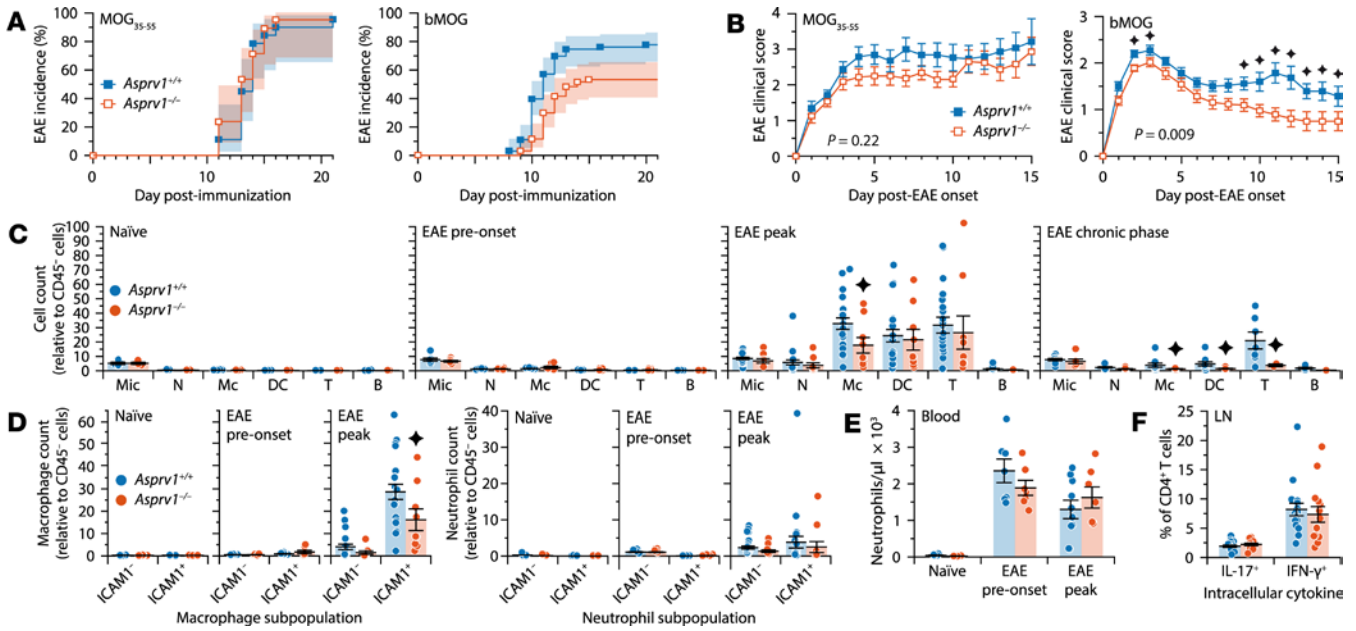

Figure 9. ASPRV1 is required for the chronic phase of EAE induced with a B cell–dependent myelin antigen (bMOG) but not for initial neutrophil recruitment or T cell priming. (**A**) Kaplan-Meier plot of EAE incidence in WT (*Asprv1*$^{+/+}$) and ASPRV1-deficient mice (*Asprv1*$^{-/-}$) after immunization with either MOG_{35-55} or bMOG. Shaded area represents the 95% pointwise CI. For sample size and statistical testing, see incidence in Table 1. (**B**) Severity of EAE over time by group versus time from appearance of first symptoms. *P* value shown on graph was calculated by 2-way ANOVA with repeated measures using rank-transformed scores. Stars indicate differences in post-hoc testing by time point (Wilcoxon test, $P < 0.0386$). Only mice that had developed EAE are included (see incidence in Table 1 for sample size). (**C**) Flow cytometric counts of immune cells in the spinal cord of *Asprv1*$^{-/-}$ and WT mice before immunization with bMOG (naive) or after at day 8 (EAE preonset), 13 (EAE peak), or 21 (EAE chronic phase). Counts were normalized to $CD45^-$ cells as an internal control. Stars indicate significant differences from *Asprv1*$^{+/+}$ mice (Wilcoxon test, $P < 0.0454$). Mic, $CD45^{lo}CD11b^+$ microglia; N, $Ly6G^+$ neutrophils; Mc, $CD45^{hi}CD11b^+CD11c^-$ macrophages; DC, $CD45^{hi}CD11b^+CD11c^+$ DCs; T, $CD3\varepsilon^+$ T cells; B, $CD19^+$ B cells. Sample size per group: 4–6 (naive), 7 (preonset), 9–22 (peak), 7–10 (chronic). (**D**) Counts of the $ICAM1^-$ (intravascular) and $ICAM1^+$ (extravascular) subpopulations of macrophages and neutrophils showing no intergroup difference, except for $ICAM1^+$ macrophages at the peak of bMOG EAE. Star indicates a significant difference from *Asprv1*$^{+/+}$ mice (Wilcoxon test, $P = 0.0374$). Sample size as in **C**. (**E**) Counts of blood neutrophils showing that bMOG immunization induces a similar mobilization of neutrophils between the genotypes. Sample size per group: 3–5 (naive), 7 (preonset), 7–10 (peak). (**F**) Proportions of Th17 ($IL\text{-}17^+$) and Th1 ($IFN\text{-}\gamma^+$) cells in inguinal lymph nodes (LN) at day 9 after immunization with bMOG, suggesting that there were no intergroup difference in T cell priming. Intracellular staining was performed on freshly collected LN cells after a 4-hour stimulation with phorbol myristate acetate and ionomycin in the presence of brefeldin A. $n = 14–17$ per group.

9E). This lower sensitivity was not attributable to a defect in T cell primin because the proportion of Th1 and Th17 cells in draining lymph nodes did not differ between the genotypes (Figure 9F), which is consistent with previous studies showing that neutrophil depletion does not affect the priming of encephalitogenic T cells (17, 35). Finally, this phenotype was only associated to ASPRV1 and not observed in mice lacking other neutrophil-specific proteins (IL-36γ and MREG; incidence, $P \geq 0.85$; day of onset, $P \geq 0.55$; severity over time, $P \geq 0.35$; $n \geq 10–12$ per group). Overall, our results demonstrate that: (i) ASPRV1 is required both to reach maximum disease severity and to sustain chronic inflammation in response to bMOG, and (ii) ASPRV1 does not significantly affect neutrophil mobilization from BM, adhesion/crawling on the CNS vasculature, or extravasation into meningeal and submeningeal compartments, which is consistent with the normal response of *Asprv1*$^{-/-}$ mice to MOG_{35-55}. Therefore, neutrophils exert, most likely in the CNS, a proinflammatory effect via ASPRV1 that is important for perpetuating inflammation specifically in a B cell–dependent form of EAE.

Discussion

The importance of neutrophils for EAE and the mechanism of their recruitment into the CNS have already been extensively investigated (6), but their phenotype and functions are largely unknown. For the first time to our knowledge, the present study: (i) identifies a surface marker (ICAM1) that distinguishes extravascular from intravascular neutrophils; (ii) identifies a neutrophil-specific marker (ASPRV1) applicable in both mice and humans within the immune and nervous systems; (iii) deciphers the transcriptomic changes undergone by neutrophils after extravasation, hence revealing functional plasticity (e.g., acquisition of macrophage-like immunostimulato-

Table 1. Statistical data on *Asprv1*$^{+/+}$ and *Asprv1*$^{+/+}$ mice immunized with either MOG_{35-55} or bMOG

	MOG_{35-55}			bMOG		
Descriptive statistics	*Asprv1*$^{+/+}$	*Asprv1*$^{-/-}$	*P*	*Asprv1*$^{+/+}$	*Asprv1*$^{-/-}$	*P*
Incidence	17/18 (94%)	16/17 (94%)	0.87	50/63 (79%)	32/60 (53%)	0.0003
Day of onset	13.7 ± 0.6	13.3 ± 0.4	0.82	11.2 ± 0.4	12.0 ± 0.5	0.021
Day at peak score	18.8 ± 1.2	19.8 ± 1.4	0.62	12.9 ±0.5	12.9 ± 0.4	0.22
Peak score	3.6 ± 0.3	3.1 ± 0.3	0.27	2.6 ± 0.1	2.1 ± 0.1	0.0020
Median score	2.4 ± 0.3	2.2 ± 0.2	0.82	0.5 ± 0.1	0.4 ± 0.1	0.91
Cumulative score	43.8 ± 5.0	40.9 ± 3.8	0.97	18.2 ± 2.1	16.8 ± 2.3	0.78
Total dead/euthanized	10/18 (56%)	3/17 (18%)	0.03	2/50 (4%)	0/32 (0%)	0.17
Full recovery	0/17 (0%)	0/16 (0%)	1.00	3/50 (6%)	10/32 (31%)	0.0040

These data were extracted from the clinical scores reported in Figure 9B. Means were compared by Fisher's exact test (for recovery), by the log-rank test (for incidence and mortality), or otherwise by Wilcoxon test.

ry and antigen presentation properties); (iv) shows in vivo that neutrophils make intimate physical contacts with T and B lymphocytes at the site of inflammation; (v) specifies the perpetuation of chronic inflammation as one context-dependent function of neutrophils; (vi) ascribes an extraepithelial role to ASPRV1 as a proinflammatory effector; and (vii) introduces a potentially novel humanized myelin antigen (bMOG) that can be used to induce a B cell–dependent form of EAE and to study neutrophil–B cell interactions.

ICAM1 as a marker for extravasated neutrophils. Under healthy conditions, neutrophils continually crawl within the CNS vasculature but do not cross the blood-brain barrier; in EAE, neutrophils become much more numerous, both continuing to patrol within blood vessels and beginning to extravasate into the meninges and parenchyma (6). Previously, when analyzing CNS samples by flow cytometry, the patrolling and infiltrating neutrophil populations could not be separated. Recent studies have reported ICAM1 expression by neutrophils under certain conditions of activation (36–38); we show here that the great majority of extravasated neutrophils in EAE express ICAM1, but not patrolling neutrophils. By allowing a better adhesion between leukocytes (e.g., via LFA1), ICAM1 facilitates cell-cell interactions such as the formation of immunological synapses (29). Our results suggest that neutrophils act, at least in part, in a contact-dependent manner in demyelination and provide a surface marker for the study of neutrophil subpopulations.

ASPRV1 as a neutrophil-specific marker in mice and humans. The Ly6G antigen conclusively identifies neutrophils in mice, but no such marker exists in humans. Those that exist (e.g., myeloperoxidase, neutrophil elastase, CD16b, and CD66b) can also be expressed by other myeloid cells and, thus, are not fully specific to neutrophils. This complicates the identification of neutrophils in human tissues (e.g., CNS), since these cells can adopt a macrophage-like phenotype and since their nucleus can be more compacted and, thus, difficult to recognize by conventional microscopy. We propose the use of ASPRV1 as a specific marker for neutrophils in human and mouse tissue samples, with the added benefit of facilitating translation of results from animal models.

Antigen-presenting function of neutrophils. Neutrophils in culture can form immunological synapses (39, 40) and present antigen to T cells (41–44), yet the relevance of these nonclassical APCs remains to be shown in vivo. We report here that neutrophils prepare for being APCs at an early stage of development by preforming *MHCII* mRNA, which can later be translated at the site of inflammation. We also provide the first in vivo evidence to our knowledge for close contacts between neutrophils and T cells within EAE lesions with a redistribution of cell-surface ICAM1. Several types of immunological synapses have been described ex vivo (29), but more characterization is required to determine to which category the synapses we observed in EAE belong. Since current genetic models cannot specifically delete MHCII in neutrophils, new strategies will be needed to confirm the importance of these synapses. For instance, neutrophils could enhance the anti-MOG Th17 response or contribute to or restrain epitope spreading by ingesting degraded myelin and presenting new epitopes to T cells in either a positive or negative regulatory manner.

ASPRV1-dependent function of neutrophils. The substrate and function of ASPRV1 were previously known only in the context of stratified epithelia (e.g., the stratum corneum of the skin), where it processes profilaggrin and enhances skin hydration (8, 9, 11, 12). We have now found that ASPRV1 is also expressed in the immune system solely by neutrophils and promotes chronic inflammation in EAE. However, the substrate of ASPRV1 in this new context is unknown, as profilaggrin and other members

of its family are not expressed in neutrophils (Supplemental Table 1) and have not been reported in the immune and nervous systems. Since ASPRV1 was ostensibly acquired from a retrotransposon sometime around the advent of mammals (45), the selective expression of ASPRV1 in neutrophils may be associated to a mammal-specific function of neutrophils. By comparison with other aspartic proteases (e.g., cathepsin D, DNA damage-inducible protein 1, pepsin, renin), ASPRV1 may be involved in an intracellular or extracellular process such as endosomal proteolysis, antigen processing for the MHCII pathway, or proteolytic activation of inflammatory mediators.

bMOG as an antigen for EAE induction. B cells contribute to MS and NMOSD in 2 major ways: by secreting autoantibodies and by stimulating the development of autoreactive Th cells via antigen presentation and secretion of cytokines (e.g., IL-6, GM-CSF, and IL-15) (46). Similarly, B cells are essential for the development of EAE when induced with either bMOG, as demonstrated herein, or human MOG protein (47). However, in the traditional $MOG_{35–55}$ model, B cells play no such role, instead acting as beneficial, regulatory cells, since depleting them exacerbates the symptoms (14, 48–57). This is possibly because DCs and macrophages can only present the immunodominant $MOG_{35–55}$ epitope to T cells, whereas B cells can process and present several epitopes, thereby mounting a more diversified response; by mutating the 35–55 epitope in bMOG, B cells become necessary APCs for T cell activation. The advantages of using bMOG are 2-fold: first, compared with the traditional MOG peptide, bMOG represents an improved model for investigating B cell–dependent responses, which is especially important given the recent success of B cell depletion therapy for MS (46); second, compared with human MOG, bMOG differs from mouse MOG by only a single amino acid, thus excluding possible confounding effects of multiple mutations and unwanted immunogenicity. Use of bMOG should help mechanistic studies of how the immune response can drift from foreign to self-epitopes.

Conclusion. Long considered a black sheep in the field of autoimmune demyelination, neutrophils should rather be seen as an essential component of a cooperative network of immune cells interacting chemically and physically with one another. By linking an ASPRV1-dependent function of neutrophils to the progression of a B cell–dependent form of EAE, our study suggests that neutrophils could be engaged in a unique way in some forms and stages of demyelinating diseases. More specifically, our study points to a possible role for neutrophils as downstream effectors of B cells in autoimmunity. Furthermore, our work provides new tools (markers, transcriptomic profiles, transgenic models, bMOG) to explore the many facets of neutrophils. In particular, ASPRV1 could prove a useful biomarker for identifying the presence of neutrophils in biological samples for basic research and clinical diagnosis. Future challenges include finding the substrate(s) of ASPRV1 in the immune system, explaining why neutrophils exert a differential effect in B cell–dependent EAE, and determining whether ASPRV1 could be targeted for the treatment of NMOSD, some forms of MS, and other immune disorders.

Methods

Human brain samples. Snap-frozen postmortem brain samples from MS and control patients were obtained from the Multiple Sclerosis Society Tissue Bank at the Imperial College London (London, United Kingdom). Additional samples from a patient with severe rebound MS activity after natalizumab withdrawal (58) was obtained from the University of Montreal Hospital Research Center. Biopsies were classified as acute active lesion (stage 1 and 2), chronic active lesion (stage 3 and 4), chronic inactive lesion (stage 5), or normal appearing white matter, as described previously (59). Lesions were scored for severity based on the degree of demyelination and inflammation, as described previously (59). Frozen sections were cut with a cryostat to obtain approximately 20 mg of tissue, which was homogenized in TRI-reagent (MilliporeSigma) and processed with the EZ-10 Spin Column Animal Total RNA Mini-prep Kit (Bio Basic) to extract RNA for qPCR. Additional sections were used for histology.

Human blood samples. Healthy volunteer blood was layered on top of lymphocyte separation medium (Wisent Bioproducts) and centrifuged for 20 minutes at 600 *g*. The top cell fraction, enriched in PBMCs, was used directly or processed with the EasySep Human $CD4^+$ T Cell, B Cell or Monocyte Isolation kits; the lower fraction, enriched with granulocytes, was processed with the EasySep Direct Human Neutrophil Isolation kit, according to the manufacturer's instructions (StemCell Technologies). RNA was purified from cell fractions using Aurum Total RNA kit (Bio-Rad).

Animals. C57BL/6, Ai6 (21), and *H2-Ab1*-floxed (33) mice were obtained from The Jackson Laboratory. *Asprv1*$^{-/-}$ (9), *Il1f9*$^{-/-}$ (25), *Mreg*$^{-/-}$ (60), and Catchup (20) mice (C57BL/6 background) were derived

from previously established colonies. B1-8 mice (61) with a homozygous deletion of the *Jκ* locus (62) were provided by Ann Haberman (Yale University, New Haven, Connecticut, USA). Genotypes were confirmed by PCR using the primers listed in Supplemental Table 5. Experiments were performed under specific pathogen-free conditions on mice aged 8–10 weeks.

bMOG production. The pET-32 MOG_{tag} vector (63) was mutated by PCR using the following primers: 5′-TACCGTCCGCCGTTTTCTCGCGTTGTTCACC-3′ and 5′-AAACGGCGGACGGTACCAGCCAACTTCCAT-3′. The resulting vector was sequenced to confirm the insertion of the S42P mutation and used to produce bMOG according to a previously described protocol (64). Final concentration was set to 5 mg/ml with no detectable impurities, as measured by Bradford assay and SDS-PAGE.

EAE induction. Mice were s.c. injected into both flanks with a total of 200 μl of emulsion containing either 300 μg of $MOG_{35–55}$ (Synpeptide) or 500 μg of bMOG (see above) dissolved in saline and mixed with an equal volume of complete Freund's adjuvant containing 500 μg of killed *Mycobacterium tuberculosis* H37 RA (Difco Laboratories). Mice were also i.p. injected with 20 μg/kg of PTX (List Biological Laboratories) immediately and 2 days after immunization.

Evaluation of EAE symptoms. Mice were weighed and scored daily as follows: 0, no visual sign of disease; 0.5, partial tail paralysis; 1, complete tail paralysis; 1.5, weakness in one hind limb; 2, weakness in both hind limbs; 2.5, partial hind limb paralysis; 3, complete hind limb paralysis; 3.5, partial forelimb paralysis; 4, complete forelimb paralysis; 5, dead or killed for humane reasons.

Flow cytometry. Blood samples were harvested by cardiac puncture in EDTA-treated cuvettes and treated with ammonium chloride solution (Stemcell Technologies) to remove erythrocytes. Mice were then anesthetized and exsanguinated by cardiac perfusion with saline. Spinal cords were harvested, minced with razor blades in Dulbecco's PBS, digested for 45 minutes at 37°C with 0.13 U/ml Liberase TM (Roche Diagnostics) and 50 U/ml DNase (MilliporeSigma) in Dulbecco's PBS, filtered through 40-μm cell strainers, and then separated from myelin debris by centrifugation at 1,000 *g* in 35% Percoll (GE Healthcare). Lymph nodes were harvested and passed through 40-μm cell strainers. For immunostaining, cells were incubated on ice for 5 minutes with rat anti-CD16/CD32 antibody (BD Biosciences, clone 2.4G2, 5 μg/ml) and Fixable Viability Dye eFluor 506 or 455UV (eBioscience, 1:1,000), then for 30 minutes with combinations of primary antibodies (Supplemental Table 6). Cells were washed and resuspended in PBS before being analyzed/sorted with a FACSAria II flow cytometer (BD Biosciences). Before analysis, the following quality control checks were performed using FlowJo (Tree Star Inc.): debris were removed using FSC-A and SSC-A, doublets were removed using FSC-A and FSC-H, and all dead cells that were positive for the fixable viability dye eFluor 455UV (eBioscience) were removed. Gates were based on fluorescence-minus-one controls. CNS cell counts were normalized to $CD45^-$ cells, whose numbers are proportional to the sample volume, to control for variation in cell yield.

ELISpot. To detect MOG-specific plasma cells in BM, 96-well plates were coated overnight at 4°C with 0.5 μg mouse $MOG_{1–125}$. Wells were blocked with 1% (wt/vol) BSA in PBS, then incubated with BM cells at 37°C with 5% CO_2. Spots were detected using a goat alkaline phosphatase-conjugated anti–mouse IgG antibody (MABTECH) and 5-bromo-4-chloro-3-indolyl-phosphate substrate (MilliporeSigma), before being counted under a dissection microscope (Leica M80).

Microarray analysis. Total RNA was extracted from FACS-purified cells using the miRNeasy Micro Kit (Qiagen). RNA (75 ng) was used to produce biotinylated single-strand cDNAs using the Affymetrix GeneChip WT Plus Reagent Kit. The cDNAs were hybridized to Affymetrix Mouse Gene 2.0 ST arrays for 16 hours at 45°C with constant rotation at 60 rpm. The arrays were washed and stained using the Affymetrix GeneChip Fluidics Station 450 and then read using the Affymetrix GeneChip Scanner 3000 7G. Data were processed using the RMA algorithm in Affymetrix Expression Console and filtered in Microsoft Excel. Using the MeV software (TIGR), filtered data (intensity > 100 in at least 1 group; SD > 100) were log_2-transformed and analyzed by hierarchical clustering using Spearman correlation. KEGG (https://david-d.ncifcrf.gov) and Ingenuity Pathway Analysis (Qiagen) were used to identify enriched pathways.

qPCR. Total RNA was extracted from cells, spinal cord, and blood using EZ-10 Spin Column Animal Total RNA Mini-preps Kit (Bio Basic), TRI-reagent (MilliporeSigma), and RNeasy Protect Animal Blood Kit (Qiagen), respectively. First strand cDNA was generated from 1–5 μg of RNA using Superscript III (Invitrogen) with random hexamers and 20-mer oligo-dT primers; it was then purified using the GenElute PCR Clean-Up Kit (MilliporeSigma). The product (20 ng) was analyzed using the LightCycler 480 system with the SYBR Green I Master mix and primers listed in Supplemental Table 7 according to the manufac-

turer's instructions (Applied Biosystems). The PCR conditions consisted of 45 cycles of denaturation (10 seconds at 95°C), annealing (10 seconds at 60°C), elongation (14 seconds at 72°C), and reading (5 seconds at 74°C). The number of mRNA copies was determined using the second derivative method (65).

Western blotting. BM cells were collected by flushing out femurs with 10 ml of HBSS (Wisent Bioproducts), filtered through 70-μm mesh, resuspended in HBSS containing 45% Percoll (GE Healthcare), and centrifuged at 1,600 *g* for 30 minutes over a 4-level Percoll density gradient (45%, 55%, 65%, 81%). Cell layers (mononuclear cells from the top and 45%–55% interface; neutrophils from the 65%–81% interface) were retrieved and lysed by sonication (3 × 5 seconds) in 50 μl RIPA buffer (50 mM Tris-HCl, 150 mM NaCl, 1% Triton X-100, 0.5% sodium deoxycholate, 0.1% SDS, 1× protease and phosphatase inhibitor cocktails [MilliporeSigma, P8340 and P5726], pH 8.0). Protein samples (20 μg) were boiled for 5 minutes in Laemmli buffer (50 mM Tris-HCl, 2% SDS, 6% β-mercaptoethanol, 10% glycerol, 12.5 μg/ml bromophenol blue), resolved on 15% SDS-polyacrylamide gel (Bio-Rad Mini-Protean II), and transferred to a polyvinylidene difluoride membrane for 45 minutes at 4°C and 100 V in transfer buffer (25 mM Tris, 200 mM glycine) containing 20% methanol. The membrane was blocked for 30 minutes at room temperature in TSM (10 mM Tris, 150 mM NaCl, 5% nonfat dry milk, 0.1% Tween 20, pH 7.4), and incubated for 1 hour at room temperature and then overnight at 4°C in 7 ml of TSM containing polyclonal rabbit antibody to ASPRV1 C-terminus (9) (1:1,000). The membrane was washed 4 times in TSM for 5 minutes and then incubated for 1 hour at room temperature with horseradish peroxidase–conjugated goat anti-rabbit antibody (111-035-144, 1:2,500; Jackson ImmunoResearch). The membrane was again washed 4 times in TSM, twice in TS (10 mM Tris, 150 mM NaCl, pH 7.4), and once briefly in water, before being incubated for 60 seconds with 1 ml Western Lightning chemiluminescence substrate (PerkinElmer); it was then blotted dry. The chemiluminescent signal was captured on Carestream Bio-Max Light Film (Kodak), which was scanned at 800 dpi and adjusted for contrast and brightness with Photoshop (Adobe). To control for protein loading, the membrane was rinsed overnight in TS and blotted for β-actin by 1-hour incubations at room temperature first in mouse anti–β-actin antibody (MAB1501, 1:5,000; Millipore, clone C4) and then in goat anti-mouse antibody (115-035-003, 1:2,500; Jackson ImmunoResearch).

Histology. Mice were transcardially perfused with saline, followed by ice-cold 4% paraformaldehyde in phosphate buffer, pH 7.4, over 10 minutes. Spinal cords were removed, postfixed for 4 hours at 4°C, and then cryoprotected overnight in 50 mM potassium phosphate-buffered saline supplemented with 20% sucrose. Series of sections were cut at 14 μm using a cryostat and stored at –20°C until analysis. Immunofluorescence was performed, as described previously (66), using combinations of primary antibodies (Supplemental Table 8). Slides were counterstained for 1 minute with 2 μg/ml DAPI and then mounted with coverslips no. 1.5H and ProLong Diamond (Molecular Probes; refractive index, 1.47). Macrophage number ($F4/80^+$) was estimated using a Stereo Investigator system (Microbrightfield) on a Nikon E800 microscope by the optical fractionator method, taking into account sampling frequency, magnification, and section thickness. To this end, inflammatory foci were traced using a ×10/0.45 objective with DAPI and sampled using a ×100/1.40 objective with the following parameters: distance between counting frames, 90 × 90 μm; frame size, 40 × 40 × 8 μm. Cells were counted if they were at least partially within the 3D counting frame and did not touch the exclusion lines.

Confocal and STED microscopy. Confocal images were acquired with a Leica TCS SP8 STED ×3 microscope (equipped with white-light laser, 405-nm diode laser, and HyD detectors) by sequential scanning using the following settings: objective, HC/PL/APO ×63/1.40 oil or ×10/0.4 dry; immersion oil, Leica Type F (refractive index, 1.518); scan speed, 600 Hz; line average, 2–4; and time gate, 0.3–6.0 ns. Laser power and gain were set to optimize signal-to-noise ratio and avoid saturation using the QLUT Glow mode. Sizes of pixel, pinhole, and *z*-step were set to optimize resolution or to oversample in the case of images to be deconvolved. STED was performed with a 775-nm depletion laser and the following adapted settings: objective, PL/APO ×100/1.40 oil STED White; line average, 6–8; time gate, 0.5–6.0 ns; STED 3D, approximately 50%–75%; and depletion laser intensity, 60% (Alexa Fluor 594) or 30% (Atto 647N). Deconvolution was performed with Huygens Professional (Scientific Volume Imaging) using a theoretical point spread function, manual settings for background intensity, and default signal-to-noise ratio. Three-dimensional reconstruction was performed with LAS X 3D Visualisation (Leica). Color balance, contrast, and brightness were adjusted with Photoshop (Adobe).

Statistics. Unless otherwise indicated, data are expressed as mean ± SEM. In general, means were compared with nonparametric (Wilcoxon, Kruskal-Wallis) or parametric tests (2-tailed Student's *t* test, 2-way

ANOVA) when data were continuous, normally distributed (Shapiro-Wilk W test), and of equal variance (Levene's test). EAE incidence curves were constructed using the Kaplan-Meier method and compared by Wilcoxon test. EAE severity curves were compared by 2-way ANOVA with repeated measures using rank-transformed scores, followed by Wilcoxon test for pairwise comparisons using untransformed scores. Correlation between variables was determined using the Spearman's or Pearson's test. All these analyses were performed with JMP (SAS Institute). A P value less than 0.05 was considered significant.

Study approval. Studies using mice and human samples were approved, respectively, by the Animal Protection Committee and the Research Ethics Committee of the University Hospital Center of Quebec – Laval University.

Author contributions

LV designed the experiments, supervised the project, and wrote the article with RFWH. RFWH, AP, and AD performed most of the experiments. RJ, YT, and SK provided bMOG and performed experiments with *B1-8*$^{+/+}$*Jκ*$^{-/-}$ mice. TM provided *Asprv1*$^{-/-}$ mice and anti-ASPRV1 antibody. MG, MP, and CL provided Catchup mice, human blood fractions, and human CNS tissues, respectively. RFWH, AP, AD, RJ, YT, SK, M, MG, PEP, CL, MP, and LV provided advice and reviewed the article.

Acknowledgments

This work was supported by grants to LV from the Multiple Sclerosis Society of Canada (MSSOC), the Canadian Institutes for Health Research, and the Natural Sciences and Engineering Research Council of Canada. RFWH and RJ were supported by MSSOC studentship awards. We thank Djordje Gveric (Multiple Sclerosis Society Tissue Bank, Imperial College London) and Kathleen Boesze-Battaglia (University of Pennsylvania) for providing human CNS tissues and *Mreg*$^{-/-}$ mice, respectively.

Address correspondence to: Luc Vallières, Neuroscience Unit, University Hospital Center of Quebec – Laval University, 2705 Laurier Boulevard, Room T2-50, Quebec City, Quebec, Canada, G1V 4G2. Phone: 418.525.4444, ext. 46233; Email: Luc.Vallieres@crchul.ulaval.ca.

1. Stromnes IM, Goverman JM. Active induction of experimental allergic encephalomyelitis. *Nat Protoc*. 2006;1(4):1810–1819.
2. Korn T, Kallies A. T cell responses in the central nervous system. *Nat Rev Immunol*. 2017;17(3):179–194.
3. Rossi B, Constantin G. Live imaging of immune responses in experimental models of multiple sclerosis. *Front Immunol*. 2016;7:506.
4. Mishra MK, Yong VW. Myeloid cells — targets of medication in multiple sclerosis. *Nat Rev Neurol*. 2016;12(9):539–551.
5. Kleinewietfeld M, Hafler DA. Regulatory T cells in autoimmune neuroinflammation. *Immunol Rev*. 2014;259(1):231–244.
6. Casserly CS, Nantes JC, Whittaker Hawkins RF, Vallières L. Neutrophil perversion in demyelinating autoimmune diseases: Mechanisms to medicine. *Autoimmun Rev*. 2017;16(3):294–307.
7. Kostic M, et al. IL-17 and glutamate excitotoxicity in the pathogenesis of multiple sclerosis. *Scand J Immunol*. 2014;79(3):181–186.
8. Bernard D, Méhul B, Thomas-Collignon A, Delattre C, Donovan M, Schmidt R. Identification and characterization of a novel retroviral-like aspartic protease specifically expressed in human epidermis. *J Invest Dermatol*. 2005;125(2):278–287.
9. Matsui T, et al. Mouse homologue of skin-specific retroviral-like aspartic protease involved in wrinkle formation. *J Biol Chem*. 2006;281(37):27512–27525.
10. Rhiemeier V, et al. A novel aspartic proteinase-like gene expressed in stratified epithelia and squamous cell carcinoma of the skin. *Am J Pathol*. 2006;168(4):1354–1364.
11. Hildenbrand M, et al. Impaired skin regeneration and remodeling after cutaneous injury and chemically induced hyperplasia in taps-transgenic mice. *J Invest Dermatol*. 2010;130(7):1922–1930.
12. Matsui T, et al. SASPase regulates stratum corneum hydration through profilaggrin-to-filaggrin processing. *EMBO Mol Med*. 2011;3(6):320–333.
13. Michel L, Touil H, Pikor NB, Gommerman JL, Prat A, Bar-Or A. B Cells in the Multiple Sclerosis Central Nervous System: Trafficking and Contribution to CNS-Compartmentalized Inflammation. *Front Immunol*. 2015;6:636.
14. Weber MS, et al. B-cell activation influences T-cell polarization and outcome of anti-CD20 B-cell depletion in central nervous system autoimmunity. *Ann Neurol*. 2010;68(3):369–383.
15. Wu F, Cao W, Yang Y, Liu A. Extensive infiltration of neutrophils in the acute phase of experimental autoimmune encephalomyelitis in C57BL/6 mice. *Histochem Cell Biol*. 2010;133(3):313–322.
16. Roy M, Richard JF, Dumas A, Vallières L. CXCL1 can be regulated by IL-6 and promotes granulocyte adhesion to brain capillaries during bacterial toxin exposure and encephalomyelitis. *J Neuroinflammation*. 2012;9:18.
17. Rumble JM, et al. Neutrophil-related factors as biomarkers in EAE and MS. *J Exp Med*. 2015;212(1):23–35.
18. Richard JF, Roy M, Audoy-Rémus J, Tremblay P, Vallières L. Crawling phagocytes recruited in the brain vasculature after pertussis toxin exposure through IL6, ICAM1 and ITGαM. *Brain Pathol*. 2011;21(6):661–671.
19. Dumas A, et al. The inflammasome pyrin contributes to pertussis toxin-induced IL-1β synthesis, neutrophil intravascular crawling and autoimmune encephalomyelitis. *PLoS Pathog*. 2014;10(5):e1004150.

20. Hasenberg A, et al. Catchup: a mouse model for imaging-based tracking and modulation of neutrophil granulocytes. *Nat Methods*. 2015;12(5):445–452.
21. Madisen L, et al. A robust and high-throughput Cre reporting and characterization system for the whole mouse brain. *Nat Neurosci*. 2010;13(1):133–140.
22. Audoy-Rémus J, Richard JF, Soulet D, Zhou H, Kubes P, Vallières L. Rod-Shaped monocytes patrol the brain vasculature and give rise to perivascular macrophages under the influence of proinflammatory cytokines and angiopoietin-2. *J Neurosci*. 2008;28(41):10187–10199.
23. Kishimoto TK, Jutila MA, Berg EL, Butcher EC. Neutrophil Mac-1 and MEL-14 adhesion proteins inversely regulated by chemotactic factors. *Science*. 1989;245(4923):1238–1241.
24. Lacal P, Pulido R, Sánchez-Madrid F, Mollinedo F. Intracellular location of T200 and Mo1 glycoproteins in human neutrophils. *J Biol Chem*. 1988;263(20):9946–9951.
25. Bozoyan L, Dumas A, Patenaude A, Vallières L. Interleukin-36γ is expressed by neutrophils and can activate microglia, but has no role in experimental autoimmune encephalomyelitis. *J Neuroinflammation*. 2015;12:173.
26. Köffel R, et al. Monocytic cell differentiation from band-stage neutrophils under inflammatory conditions via MKK6 activation. *Blood*. 2014;124(17):2713–2724.
27. Ohsawa K, Imai Y, Kanazawa H, Sasaki Y, Kohsaka S. Involvement of Iba1 in membrane ruffling and phagocytosis of macrophages/microglia. *J Cell Sci*. 2000;113(pt 17):3073–3084.
28. Neumann J, et al. Very-late-antigen-4 (VLA-4)-mediated brain invasion by neutrophils leads to interactions with microglia, increased ischemic injury and impaired behavior in experimental stroke. *Acta Neuropathol*. 2015;129(2):259–277.
29. Friedl P, den Boer AT, Gunzer M. Tuning immune responses: diversity and adaptation of the immunological synapse. *Nat Rev Immunol*. 2005;5(7):532–545.
30. Yuseff MI, Pierobon P, Reversat A, Lennon-Duménil AM. How B cells capture, process and present antigens: a crucial role for cell polarity. *Nat Rev Immunol*. 2013;13(7):475–486.
31. Barcia C, et al. In vivo mature immunological synapses forming SMACs mediate clearance of virally infected astrocytes from the brain. *J Exp Med*. 2006;203(9):2095–2107.
32. Barcia C, et al. T cells' immunological synapses induce polarization of brain astrocytes in vivo and in vitro: a novel astrocyte response mechanism to cellular injury. *PLoS One*. 2008;3(8):e2977.
33. Hashimoto K, Joshi SK, Koni PA. A conditional null allele of the major histocompatibility IA-beta chain gene. *Genesis*. 2002;32(2):152–153.
34. Hjelmström P, Juedes AE, Fjell J, Ruddle NH. B-cell-deficient mice develop experimental allergic encephalomyelitis with demyelination after myelin oligodendrocyte glycoprotein sensitization. *J Immunol*. 1998;161(9):4480–4483.
35. Steinbach K, Piedavent M, Bauer S, Neumann JT, Friese MA. Neutrophils amplify autoimmune central nervous system infiltrates by maturing local APCs. *J Immunol*. 2013;191(9):4531–4539.
36. Yao Y, Matsushima H, Ohtola JA, Geng S, Lu R, Takashima A. Neutrophil priming occurs in a sequential manner and can be visualized in living animals by monitoring IL-1β promoter activation. *J Immunol*. 2015;194(3):1211–1224.
37. Woodfin A, et al. ICAM-1-expressing neutrophils exhibit enhanced effector functions in murine models of endotoxemia. *Blood*. 2016;127(7):898–907.
38. Heemskerk N, Asimuddin M, Oort C, van Rijssel J, van Buul JD. Annexin A2 Limits Neutrophil Transendothelial Migration by Organizing the Spatial Distribution of ICAM-1. *J Immunol*. 2016;196(6):2767–2778.
39. Pillay J, et al. A subset of neutrophils in human systemic inflammation inhibits T cell responses through Mac-1. *J Clin Invest*. 2012;122(1):327–336.
40. Vono M, Lin A, Norrby-Teglund A, Koup RA, Liang F, Loré K. Neutrophils acquire the capacity for antigen presentation to memory CD4(+) T cells in vitro and ex vivo. *Blood*. 2017;129(14):1991–2001.
41. Okuda K, Tani K, Ishigatsubo Y, Yokota S, David CS. Antigen-pulsed neutrophils bearing Ia antigens can induce T lymphocyte proliferative response to the syngeneic or semisyngeneic antigen-primed T lymphocytes. *Transplantation*. 1980;30(5):368–372.
42. Culshaw S, Millington OR, Brewer JM, McInnes IB. Murine neutrophils present Class II restricted antigen. *Immunol Lett*. 2008;118(1):49–54.
43. Abi Abdallah DS, Egan CE, Butcher BA, Denkers EY. Mouse neutrophils are professional antigen-presenting cells programmed to instruct Th1 and Th17 T-cell differentiation. *Int Immunol*. 2011;23(5):317–326.
44. Ostanin DV, et al. Acquisition of antigen-presenting functions by neutrophils isolated from mice with chronic colitis. *J Immunol*. 2012;188(3):1491–1502.
45. Strasser B, Mlitz V, Fischer H, Tschachler E, Eckhart L. Comparative genomics reveals conservation of filaggrin and loss of caspase-14 in dolphins. *Exp Dermatol*. 2015;24(5):365–369.
46. Li R, et al. Cytokine-Defined B Cell Responses as Therapeutic Targets in Multiple Sclerosis. *Front Immunol*. 2015;6:626.
47. Oliver AR, Lyon GM, Ruddle NH. Rat and human myelin oligodendrocyte glycoproteins induce experimental autoimmune encephalomyelitis by different mechanisms in C57BL/6 mice. *J Immunol*. 2003;171(1):462–468.
48. Wolf SD, Dittel BN, Hardardottir F, Janeway CA. Experimental autoimmune encephalomyelitis induction in genetically B cell-deficient mice. *J Exp Med*. 1996;184(6):2271–2278.
49. Dittel BN, Urbania TH, Janeway CA. Relapsing and remitting experimental autoimmune encephalomyelitis in B cell deficient mice. *J Autoimmun*. 2000;14(4):311–318.
50. Fillatreau S, Sweenie CH, McGeachy MJ, Gray D, Anderton SM. B cells regulate autoimmunity by provision of IL-10. *Nat Immunol*. 2002;3(10):944–950.
51. Lyons JA, Ramsbottom MJ, Mikesell RJ, Cross AH. B cells limit epitope spreading and reduce severity of EAE induced with PLP peptide in BALB/c mice. *J Autoimmun*. 2008;31(2):149–155.
52. Lehmann-Horn K, et al. Anti-CD20 B-cell depletion enhances monocyte reactivity in neuroimmunological disorders. *J Neuroinflammation*. 2011;8:146.
53. Matsushita T, et al. Inhibitory role of CD19 in the progression of experimental autoimmune encephalomyelitis by regulating cytokine response. *Am J Pathol*. 2006;168(3):812–821.

54. Matsushita T, Yanaba K, Bouaziz JD, Fujimoto M, Tedder TF. Regulatory B cells inhibit EAE initiation in mice while other B cells promote disease progression. *J Clin Invest*. 2008;118(10):3420–3430.
55. Matsushita T, Horikawa M, Iwata Y, Tedder TF. Regulatory B cells (B10 cells) and regulatory T cells have independent roles in controlling experimental autoimmune encephalomyelitis initiation and late-phase immunopathogenesis. *J Immunol*. 2010;185(4):2240–2252.
56. Ray A, Mann MK, Basu S, Dittel BN. A case for regulatory B cells in controlling the severity of autoimmune-mediated inflammation in experimental autoimmune encephalomyelitis and multiple sclerosis. *J Neuroimmunol*. 2011;230(1–2):1–9.
57. Ray A, Basu S, Williams CB, Salzman NH, Dittel BN. A novel IL-10-independent regulatory role for B cells in suppressing autoimmunity by maintenance of regulatory T cells via GITR ligand. *J Immunol*. 2012;188(7):3188–3198.
58. Larochelle C, et al. Immunological and pathological characterization of fatal rebound MS activity following natalizumab withdrawal. *Mult Scler*. 2017;23(1):72–81.
59. Reynolds R, Roncaroli F, Nicholas R, Radotra B, Gveric D, Howell O. The neuropathological basis of clinical progression in multiple sclerosis. *Acta Neuropathol*. 2011;122(2):155–170.
60. Rachel RA, et al. Melanoregulin, product of the dsu locus, links the BLOC-pathway and OA1 in organelle biogenesis. *PLoS One*. 2012;7(9):e42446.
61. Maruyama M, Lam KP, Rajewsky K. Memory B-cell persistence is independent of persisting immunizing antigen. *Nature*. 2000;407(6804):636–642.
62. Chen J, et al. Immunoglobulin gene rearrangement in B cell deficient mice generated by targeted deletion of the JH locus. *Int Immunol*. 1993;5(6):647–656.
63. Dang AK, Jain RW, Craig HC, Kerfoot SM. B cell recognition of myelin oligodendrocyte glycoprotein autoantigen depends on immunization with protein rather than short peptide, while B cell invasion of the CNS in autoimmunity does not. *J Neuroimmunol*. 2015;278:73–84.
64. Jain RW, Dang AK, Kerfoot SM. Simple and efficient production and purification of mouse myelin oligodendrocyte glycoprotein for experimental autoimmune encephalomyelitis studies. *J Vis Exp*. 2016;(116):e54727.
65. Luu-The V, Paquet N, Calvo E, Cumps J. Improved real-time RT-PCR method for high-throughput measurements using second derivative calculation and double correction. *BioTechniques*. 2005;38(2):287–293.
66. Vallières L, Sawchenko PE. Bone marrow-derived cells that populate the adult mouse brain preserve their hematopoietic identity. *J Neurosci*. 2003;23(12):5197–5207.